Chemical Science

Accepted Manuscript

This article can be cited before page numbers have been issued, to do this please use: Z. Bai, J. Luo and K. M. Ok, *Chem. Sci.*, 2026, DOI: 10.1039/D6SC03331H.

ROYAL SOCIETY OF CHEMISTRY

rsc.li/chemical-science

View Article Online
DOI: 10.1039/D6SC03331H

Hybridizing π-conjugated organic systems with tetrahedral units: a design paradigm for advanced UV nonlinear optical materials

Zhiyong Bai,[2] Junhua Luo,[2*] Kang Min Ok[1*]

[1]Department of Chemistry, Sogang University, 35 Baekbeom-ro, Mapo-gu, Seoul 04107, Korea;

[2]State Key Laboratory of Functional Crystals and Devices, Fujian Institute of Research on the Structure of Matter, Chinese Academy of Sciences, Fuzhou, Fujian 350002, China;

jhluo@fjirsm.ac.cn; kmok@sogang.ac.kr

Abstract: Ultraviolet (UV) nonlinear optical (NLO) materials are essential for modern laser technologies; however, the development of new materials that simultaneously exhibit wide band gaps, large second-harmonic generation (SHG) responses, and sufficient birefringence remains a major challenge attributed to intrinsic property trade-offs. This Perspective highlights a synergistic design strategy that integrates organic π-conjugated systems with inorganic tetrahedral units to overcome these limitations. We systematically review recent advances in three representative hybrid material systems: guanidinium-, melamine-, and 4-hydroxypyridine-based compounds. The deliberate assembly of these complementary building blocks enables the simultaneous optimization of key optical properties, including broad UV transparency, strong SHG responses, and tunable birefringence. We further discuss underlying structure-property relationships and outline future research directions, emphasizing that chemical modification of π-conjugated systems offers a promising pathway for the rational design of next-generation UV NLO materials.

View Article Online
DOI: 10.1039/D6SC03331H

1. Introduction

Ultraviolet (UV) nonlinear optical (NLO) materials are indispensable for modern photonics, particularly for generating 266 nm coherent light through direct fourth-harmonic generation of widely used 1064 nm laser sources.[1-5] These materials play a pivotal role in semiconductor manufacturing, precision micromachining, and advanced laser technologies. Promising UV NLO candidates must satisfy several stringent structural and physicochemical requirements. From a structural standpoint, candidate materials must crystallize in one of the 16 noncentrosymmetric (NCS) crystal classes, which are necessary for second-order NLO responses. These includes five biaxial point groups (1, *m*, 2, *mm*2, and 222), corresponding to 39 NCS space group, and 11 uniaxial point groups (4, 4, 4*mm*, 42*m*, 3, 3*m*, 62*m*, 6*mm*, 32, 6, and 6), corresponding to 74 NCS space groups. From an optical perspective, target materials should exhibit high transparency at 266 nm, along with a wide optical band gap (E_g) and a short UV cutoff edge (λ_{cutoff}). In addition, they must possess a large second-harmonic generation (SHG) coefficient, combined with sufficient birefringence (ideally Δn = 0.05–0.1) and low optical dispersion to enable short phase-matching wavelengths (λ_{PM}). From a practical standpoint, UV NLO materials should also demonstrate robust physicochemical stability, high laser-induced damage thresholds (LIDTs), and the ability to grow as large, high-quality single-crystals. To date, only a limited number of UV NLO crystals have been commercialized, including β-BaB_2O_4 (β-BBO),[6] LiB_3O_5 (LBO),[7] $CsLiB_6O_{10}$(CLBO),[8] CsB_3O_5 (CBO),[9] and $KBe_2BO_3F_2$ (KBBF),[10] the latter being particularly important for generating coherent light below 200 nm. Despite their advantages, these materials suffer from intrinsic limitations. Therefore, the development of new UV NLO materials with improved performance remains a pressing challenge.

Among the stringent criteria for high-performance UV NLO materials, a short UV cutoff edge, a large SHG coefficient, and sufficient birefringence are identified as the three most pivotal performance metrics. Accordingly, the design of advanced UV NLO crystals fundamentally requires achieving a delicate balance among these three

View Article Online
DOI: 10.1039/D6SC03331H

parameters. However, intrinsic trade-offs among these properties present significant challenges for both design and synthesis. An effective strategy to address this challenge is the synergistic integration of covalent tetrahedral units with planar π-conjugated groups. Tetrahedral units typically provide broad UV transparency (characterized by wide E_g and short λ_{cutoff}) and low optical dispersion, which are beneficial for optimizing the λ_{PM}. In contrast, planar π-conjugated units offer strong polarizability anisotropy and large hyperpolarizability, thereby enhancing birefringence and SHG performance. A representative example is the well-known KBBF crystal, in which $[BeO_3F]$ tetrahedra eliminate dangling bonds associated with terminal oxygen atoms in the π-conjugated $[BO_3]^{3-}$ units. This structural feature enables an exceptionally short UV cutoff edge while preserving large birefringence and a high SHG coefficient. The success of KBBF has stimulated extensive research into the design of inorganic UV NLO crystals through the combination of diverse tetrahedral motifs with π-conjugated units, leading to the development of materials such as $Ba_3Mg_3(BO_3)_3F_3$, $NH_4B_4O_6F$, $CsZn_2BO_3FCl$, and $NaZnCO_3(OH)$, among others.[11-18]

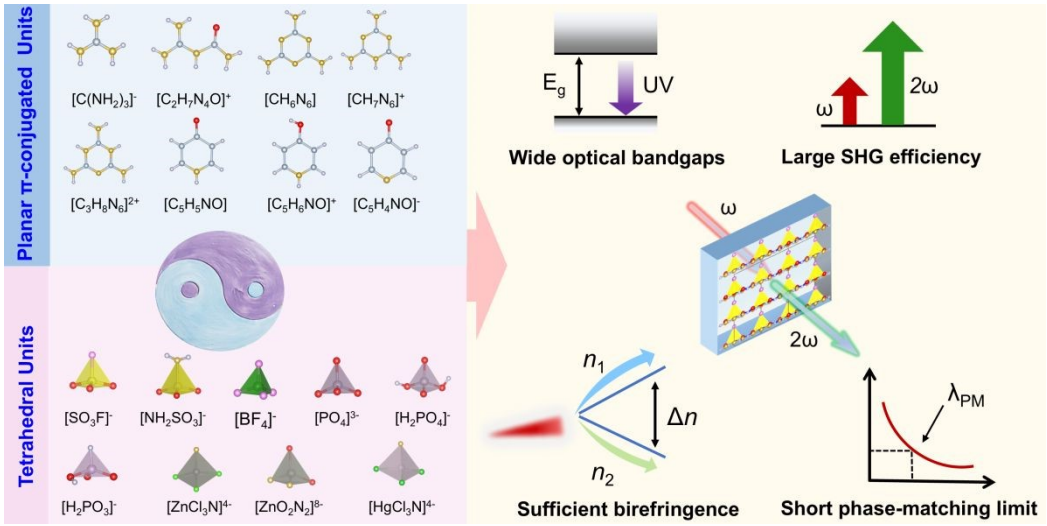

Scheme 1. Synergistic integration of organic π-conjugated units with inorganic tetrahedral modules enables UV NLO crystals exhibiting wide optical band gaps, strong SHG responses, sufficient birefringence, and short phase-matching wavelengths.

View Article Online
DOI: 10.1039/D6SC03331H

However, the library of inorganic π-conjugated building blocks remains limited, consisting primarily of $[BO_3]^{3-}$, $[CO_3]^{2-}$, $[NO_3]^-$, and $[B_3O_6]^{3-}$ units. In contrast, organic π-conjugated units[19] not only offer far greater structural diversity and chemical tunability but, more importantly, exhibit higher polarizability anisotropy (α) and hyperpolarizability ($|\beta_{max}|$) than their inorganic counterparts (Figure 1). These features make organic π-conjugated systems highly attractive candidates for hybridization with tetrahedral units in the rational design of UV NLO crystals. The deliberate integration of these two complementary building blocks—tetrahedral inorganic units and organic π-conjugated cations—provides a promising strategy to balance the key performance requirements for UV applications, namely strong SHG responses, broad UV transparency windows, large birefringence, and short phase-matching wavelengths (Scheme 1). In addition, materials based on this hybrid design concept can often be grown as large, high-quality single crystals using solution-based methods, offering clear advantages in scalability, processability, and energy efficiency compared with conventional high-temperature solid-state routes. In this context, significant progress has been achieved in three representative material systems: guanidinium-, pyridine-, and melamine-based UV NLO crystals. This Perspective aims to provide a systematic overview of recent advances in this hybrid design strategy, with an emphasis on structural motifs, key optical properties, structure-property relationships, and future opportunities.

View Article Online
DOI: 10.1039/D6SC03331H

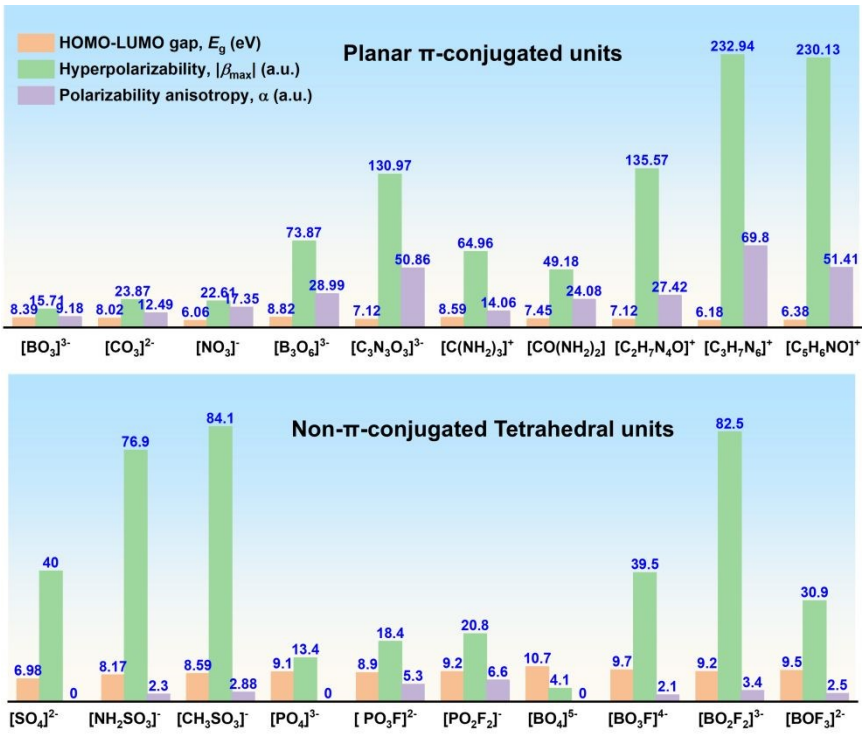

Figure 1. Basic electronic properties of commonly used building units for UV NLO materials, including the HOMO-LUMO energy gap (E_g), the absolute value of the maximum hyperpolarizability tensor ($|\beta_{max}|$), and the polarizability anisotropy (α) of planar π-conjugated units and non-π-conjugated tetrahedral units. HOMO: highest occupied molecular orbital; LUMO: lowest unoccupied molecular orbital. All data are collected from references.[20-24]

View Article Online
DOI: 10.1039/D6SC03331H

Table 1. Crystallographic symmetry, tetrahedral building units, SHG response, birefringence (Δn), band gap (E_g), UV cutoff edge (λ_{cutoff}), and UV phase-matching limit (λ_{PM}) of selected UV NLO crystals consisting of planar π-conjugated organic groups (guanidinium, melamine, 4-hydroxylpyridine, and their derivatives) and various tetrahedral units.

Compounds	Space group	Tetrahedron	SHG	Δn	E_g (eV)	λ_{cutoff} (nm)	λ_{PM} (nm)
$C(NH_2)_3SO_3F$[25]	*R*3*m*	$[SO_3F]^-$	5 × KDP[a] 0.7 × β-BBO[b]	0.133@1064 nm[d]	6.2	200[i]	200
$[C(NH_2)_3][B_3O_3F_2(OH)_2]$[26]	*P*1	$[BO_2F_2]^{3-}$	0.9 × KDP[a] 0.3 × β-BBO[b]	0.173@1064 nm[d]	6.53	190[i]	190
$[C(NH_2)_3]_2[B_3O_3F_4(OH)]$[26]	*P*1	$[BO_2F_2]^{3-}$	1.4 × KDP[a] 0.5 × β-BBO[b]	0.161@1064 nm[d]	6.36	195[i]	195
$[C(NH_2)_3]_6(PO_4)_2\square 3H_2O$[27]	*Cc*	$[PO_4]^{3-}$	3.8 × KDP[a] 0.3 × β-BBO[b]	0.077@546 nm[d] 0.078@546 nm[e]	6.05	205[j]	250
$(C_2H_7N_4O)(H_2PO_3)$[28]	*Cc*	$[H_2PO_3]^-$	2.2 × KDP[a] 1.0 × β-BBO[b]	0.19@589.3 nm[g] 0.195@546 nm[d]	5.77[h]	215[j]	215
$(C_2H_7N_4O)(NH_2SO_3)$[21]	*P*1	$[NH_2SO_3]^-$	6.2 × KDP[a]	0.225@1064 nm[d] 0.239@546 nm[d]	5.46[h]	227[j]	227
$C(NH_2)_3BF_4$[29]	*R*3*m*	$[BF_4]^-$	$\lvert d_{22}\rvert$ = 1.22 pm/V[c] $\lvert d_{15}\rvert$ = 0.76 pm/V[c]	0.120@546 nm[f]	6.42[h]	193[j]	194
$(C_3H_7N_6)(C_3H_6N_6)ZnCl_3$[22]	$P2_1$	$[ZnCl_3N]^{4-}$	2.8 × KDP[a]	0.255@1064 nm[d]	N.A.	236[i]	N.A.
$(C_3H_7N_6)(C_3H_6N_6)HgCl_3$[30]	$P2_1$	$[HgCl_3N]^{4-}$	5 × KDP[a]	0.246@1064 nm[d]	4.40	278[i]	N.A.
α-$C_3H_8N_6(BF_4)_2\cdot H_2O$[31]	*Cc*	$[BF_4]^-$	6.4 × KDP[a] 1.4 × β-BBO[b]	0.102@546.1 nm[e]	4.96[h]	250[j]	N.A.
$(C_5H_6ON)(H_2PO_4)$[20]	$P2_12_12_1$	$[H_2PO_4]^-$	3 × KDP[a]	0.25@1064 nm[d]	4.69	N.A.	266

View Article Online
DOI: 10.1039/D6SC03331H

$(C_5H_6NO)(CH_3SO_3)$[32]	*Pna*2$_1$	$[CH_3SO_3]^-$	3.3 × KDP[a]	0.202@546 nm[d] 0.198@589.3 nm[d] 0.216@546 nm[e] 0.210@589.3 nm[g]	4.64	252[j]	N.A.
$Zn(C_5H_4NO)_2$[33]	*Fdd*2	$[ZnO_2N_2]^{8-}$	13.6 × KDP[a]	0.073@532 nm[d]	4.40	N.A.	N.A.

[a] SHG intensity at 1064 nm measured by the Kurtz-Perry method; [b] SHG intensity at 532 nm measured by the Kurtz-Perry method; [c] SHG coefficients at 1064 nm measured by the Maker fringe method; [d] Δn calculated by DFT; [e] Δn experimentally determined using a polarizing microscope; [f] Δn experimentally determined by the minimum deviation method; [g] Δn experimentally determined by the immersion technique. [h] E_g values estimated from λ_{cutoff} values using the equation $E_g = 1240/\lambda_{cutoff}$, where only the λ_{cutoff} values obtained from transmittance spectra of single crystals were used; [i] λ_{cutoff} determined from diffuse-reflectance spectra of powdered samples; [j] λ_{cutoff} determined from transmittance spectra of single crystals. Note that all listed E_g and λ_{cutoff} values are experimental data, whereas all λ_{PM} are theoretically predicted.

2. UV NLO crystals assembled from guanidium and tetrahedral units

Guanidinium, $[C(NH_2)_3]^+$, has attracted significant interest in the design of UV NLO materials owing to several key attributes. First, it is structurally analogous to classical inorganic π-conjugated triangular units such as $[BO_3]^{3-}$, $[CO_3]^{2-}$, and $[NO_3]^-$, and possesses a delocalized electronic structure that gives rise to large hyperpolarizability and strong polarizability anisotropy. These features contribute substantially to enhanced SHG responses and sufficient birefringence in the resulting crystals. Second, its wide energy band gap enables solar-blind UV and even deep-UV transparency. Third, guanidium readily forms stable ionic crystals through strong electrostatic interactions and extensive hydrogen-bonding networks with a variety of inorganic anions. Collectively, these characteristics establish guanidinium as a versatile and effective π-conjugated cation for the rational design of high-performance UV NLO materials. Indeed, its combination with diverse tetrahedral units has led to a series of UV-transparent functional crystals exhibiting strong SHG responses, large birefringence, wide optical bandgap, and short phase-matching wavelengths.

The combination of $[C(NH_2)_3]^+$ with fluorine-containing tetrahedral anions, such as $[PO_3F]^{2-}$, $[SO_3F]^-$, and fluoroborate-related units, has yielded several representative NLO crystals, including $[[C(NH_2)_3]_2PO_3F$, $C(NH_2)_3SO_3F$, $[C(NH_2)_3][B_3O_3F_2(OH)_2]$, and $[C(NH_2)_3]_2[B_3O_3F_4(OH)]$.[25, 26, 34] These compounds exhibit favorable NLO

properties. For example, the fluorooxoborates $[C(NH_2)_3][B_3O_3F_2(OH)_2]$ and $[C(NH_2)_3]_2[B_3O_3F_4(OH)]$ show good UV transparency, relatively large SHG responses, sufficient birefringence, and very short phase-matching wavelengths extending below 200 nm. However, their low crystallographic symmetry (space group *P*1) may present challenges for practical applications. Among these compounds, $C(NH_2)_3SO_3F$ exhibits superior comprehensive NLO performance. $C(NH_2)_3SO_3F$ was first reported by Luo et al. through the incorporation of $[C(NH_2)_3]^+$ cations with fluoroxosulfate $[SO_3F]^-$ tetrahedra.[25] Its design was inspired by the well-known deep-UV NLO crystal $KBe_2BO_3F_2$ (KBBF), serving as a structural template in which the planar organic $[C(NH_2)_3]^+$ units and inorganic $[SO_3F]^-$ tetrahedra replace the $[BO_3]^{3-}$ and $[BeO_3F]^{5-}$ units, respectively (Figure 2). The extensive hydrogen-bonding interactions between $[C(NH_2)_3]^+$ and $[SO_3F]^-$units give rise to unique $[C(NH_2)_3SO_3F]$ layers, which topologically resemble the $[Be_2BO_3F_2]$ layers in KBBF. Benefiting from its polar crystal structure (space group: *R*3*m*) and KBBF-like architecture, both the $[C(NH_2)_3]^+$ triangular units and $[SO_3F]^-$ tetrahedra adopt a highly ordered and uniform alignment. According to anionic group theory, such an arrangement enables constructive superposition of microscopic second-order polarizabilities, ultimately resulting in a large macroscopic NLO response. Powder SHG measurements confirm a strong SHG intensity of 5 × KDP at 1064 nm and 0.7 × β-BBO @532 nm for $C(NH_2)_3SO_3F$. Thermogravimetric analysis reveals that $C(NH_2)_3SO_3F$ is thermally stable up to 162 °C. Theoretical calculations further reveal that the π-conjugated $[C(NH_2)_3]^+$ units contribute ~81% of the total SHG response, highlighting their dominant role in generating the enhanced NLO effect. In addition, the coplanar arrangement and pronounced polarizability anisotropy of the $[C(NH_2)_3]^+$ units give rise to a relatively large birefringence (Δn = 0.133 @1064 nm), which enables a short phase-matching limit down to 200 nm. Collectively, these outstanding properties position $C(NH_2)_3SO_3F$ as a promising, nontoxic, and cost-effective candidate for advanced UV NLO applications.

View Article Online
DOI: 10.1039/D6SC03331H

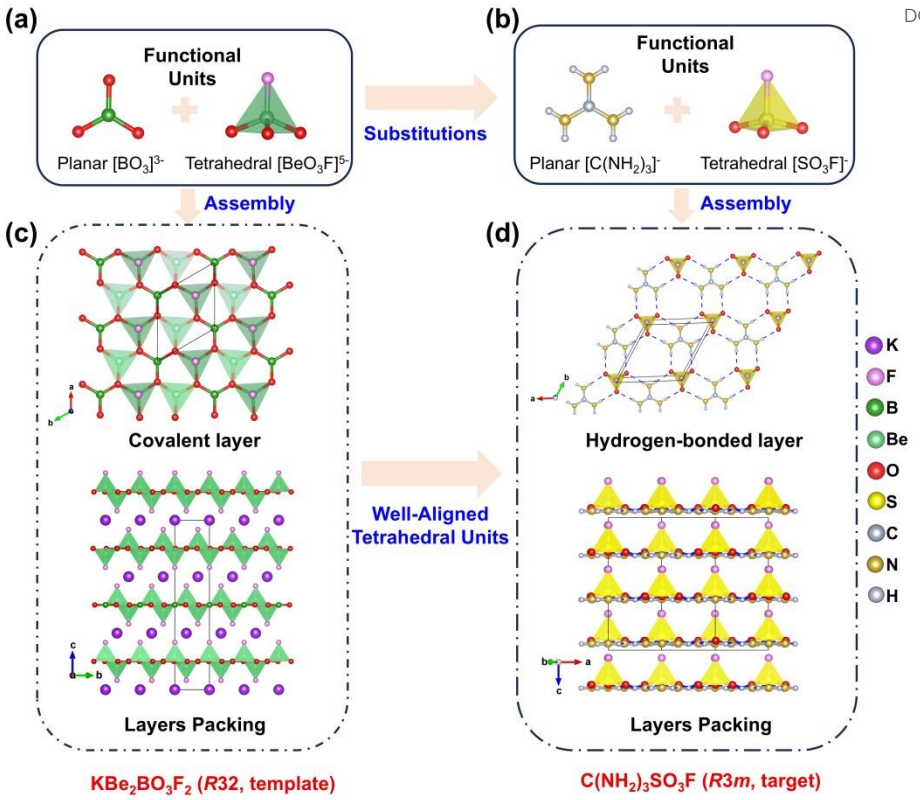

Figure 2. Structural evolution from $KBe_2BO_3F_2$ (KBBF) to $C(NH_2)_3SO_3F$. Functional building units of (a) KBBF and (b) $C(NH_2)_3SO_3F$, and (c, d) their corresponding crystal structures.

Additional guanidinium-based UV NLO materials have been developed by combining $[C(NH_2)_3]^+$ with non-fluorinated tetrahedral anions, including $[C(NH_2)_3]_6(PO_4)_2\cdot 3H_2O$,[27] $[C(NH_2)_3]_3(AsO_4)\cdot 2H_2O$,[35] and $[C(NH_2)_3]_3(VO_4)\cdot 2H_2O$.[36] Among these, $[C(NH_2)_3]_6(PO_4)_2\cdot 3H_2O$ stands out attributable to its strong SHG response, moderate birefringence, and favorable phase-matching behavior. Small single crystals of this compound were readily obtained via a facile aqueous solution evaporation method. Crystallizing in the polar space group *Cc*, $[C(NH_2)_3]_6(PO_4)_2\cdot 3H_2O$ features a three-dimensional (3D) framework constructed from π-conjugated $[C(NH_2)_3]^+$ cations, $[PO_4]^{3-}$ tetrahedra, and lattice water molecules interconnected through extensive hydrogen bonding (Figure 3). Notably, six $[C(NH_2)_3]^+$ planar triangular units exhibit a high degree of orientational alignment along the *c* axis, which in turn directs the alignment of the $[PO_4]^{3-}$ tetrahedra via hydrogen-bonding interactions. This cooperative structural arrangement significantly enhances both optical anisotropy

and SHG response. The compound exhibits a short UV cutoff edge at 205 nm and a wide band gap exceeding 6.0 eV. SHG measurements reveal strong responses of 3.8 × KDP at 1064 nm and 0.3 × β-BBO at 532 nm. The birefringence is measured to be Δn = 0.078 at 546 nm using a polarizing microscope, resulting in a phase-matching limit extending to 250 nm. It was found that $[C(NH_2)_3]_6(PO_4)_2 \cdot 3H_2O$ begins to decompose at approximately 100 °C due to the release of lattice water molecules. Theoretical real-space atom-cutting analyses indicate that the dominant contributions to both SHG and birefringence originate from the $[C(NH_2)_3]^+$ cations (accounting for 60.2% of the largest SHG coefficient, d_{33}, and 54.4% of the birefringence at 546 nm), while the $[PO_4]^{3-}$ tetrahedra provide secondary contributions.

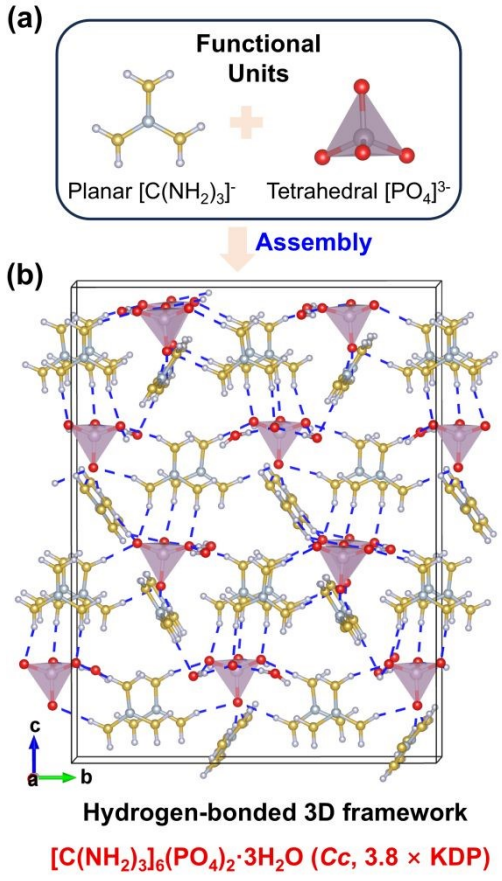

Figure 3. Crystal structure of $[C(NH_2)_3]_6(PO_4)_2 \cdot 3H_2O$. (a) Planar $[C(NH_2)_3]^+$ and tetrahedral $[PO_4]^{3-}$ building units. (b) Hydrogen-bonded 3D framework.

The demonstrated effectiveness of guanidinium-based building blocks in achieving favorable UV NLO properties has motivated researchers to further expand

the chemical space and property tunability of this materials family by exploring new guanidinium-derived units. Among these, N-carbamoylguanidium ($[C_2H_7N_4O]^+$) exhibits higher polarizability anisotropy and hyperpolarizability than guanidium, while maintaining a suitable energy gap (Figure 4a, b), highlighting its potential for designing UV NLO materials with enhanced performance.[21, 28] Pan and co-workers introduced the $[C_2H_7N_4O]^+$ unit into a phosphite framework to synthesize $[C_2H_7N_4O]H_2PO_3$.[28] The structure consists of π-conjugated cations interconnected with tetrahedral $[H_2PO_3]^-$ anions through extensive hydrogen-bonding networks (Figure 4c). This compound exhibits strong SHG responses of 2.2 × KDP at 1064 nm and 1.0 × β-BBO at 532 nm, supported by a calculated SHG coefficient of $|d_{11}|$ = 1.57 pm/V. Thermogravimetric analysis further indicates that $[C_2H_7N_4O]H_2PO_3$ is thermally stable up to 182 °C. Theoretical analyses indicate that the π-conjugated cations dominate both the birefringence and SHG response, while the $[H_2PO_3]^-$ anions primarily serve as structural scaffolds through hydrogen bonding without compromising UV transparency. Notably, $[C_2H_7N_4O]H_2PO_3$ exhibits a large birefringence of Δn = 0.19 at 589.3 nm, enabling phase-matching across a broad transparency window (215–1600 nm). Peng et al. reported another promising UV NLO crystal, $[C_2H_7N_4O]NH_2SO_3$ (Figure 4d),[21] synthesized by combining $[C_2H_7N_4O]^+$ with the sulfonate tetrahedral anion, $[NH_2SO_3]^-$. The favorable alignment of both cationic and anionic units within the crystal structures yields a strong SHG response of 6.2 × KDP at 1064 nm. Compared with previously reported guanidinium-based UV NLO crystals, $[C_2H_7N_4O]NH_2SO_3$ exhibits a significantly larger birefringence (Δn = 0.225 at 1064 nm), enabling phase-matching down to 227 nm. In addition, $[C_2H_7N_4O]NH_2SO_3$ exhibits relatively high thermal stability up to 205 °C. This characteristic makes it particularly suitable for generating UV laser output, such as the 266 nm emission obtained from fourth-harmonic generation of Nd:YAG lasers. Theoretical studies further confirm that the $[C_2H_7N_4O]^+$ cations are the primary contributors to both the enhanced SHG response and large birefringence.

View Article Online
DOI: 10.1039/D6SC03331H

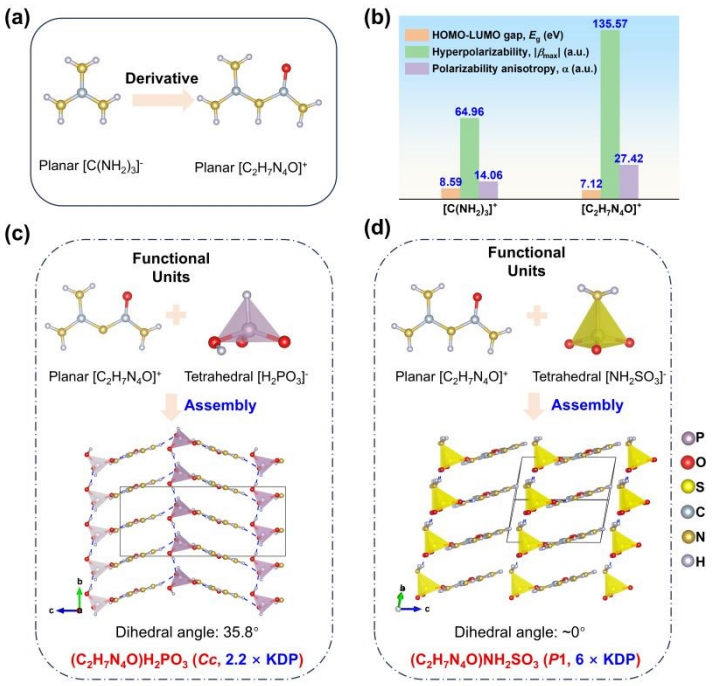

Figure 4. Crystal structures of $(C_2H_7N_4O)H_2PO_3$ and $(C_2H_7N_4O)NH_2SO_3$. (a) Planar $[C_2H_7N_4O]^+$ unit derived from $[C(NH_2)_3]^+$. (b) Comparison of the energy gap maximum hyperpolarizability, and polarizability anisotropy of $[C(NH_2)_3]^+$ and $[C_2H_7N_4O]^+$ units.[21] Functional building units and crystal structures of (c) $(C_2H_7N_4O)H_2PO_3$ and (d) $(C_2H_7N_4O)NH_2SO_3$.

These findings underscore that integrating π-conjugated guanidinium and its derivatives with diverse tetrahedral units constitutes a promising strategy for developing advanced UV NLO materials. Such materials can not only achieve an optimal balance among the three critical performance metrics such as large SHG responses, sufficient birefringence, and short UV cut-off edges, but, more importantly, can exhibit exceptional phase-matching capability essential for practical applications. These insights highlight the strong potential of guanidium-based compounds for real-word utilization. To realize this potential, the growth of large, high quality single crystals is of paramount importance for comprehensive evaluation of their intrinsic pysico-chemical and optical properties. This includes precise determination of refractive indices, phase-matching ranges and angles, SHG coefficients, and laser-induced damage thresholds (LIDTs), as well as the execution of laser output experiments. In this context, Pan et al. recently reported the growth of large single

View Article Online
DOI: 10.1039/D6SC03331H

crystals, detailed property characterization, and laser performance of a NCS guanidinium tetrahedrafluoroborate, $[C(NH_2)_3]BF_4$.[29] This compound is isostructural with $[C(NH_2)_3]SO_3F$ and features a unique layered architecture composed of π-conjugated $[C(NH_2)_3]^+$ planar triangles and $[BF_4]^-$ tetrahedra interconnected through hydrogen bonding (Figure 5), a structural feature that underpins its exceptional NLO properties. Large, high-quality single crystals (up to $40 \times 30 \times 21$ mm^3) can be readily grown from aqueous solution, providing a solid foundation for comprehensive optical characterization and laser experiments. $[C(NH_2)_3]BF_4$ exhibits a short UV cutoff edge at 193 nm and a broad transparency window (>80% transmittance from 220 to 1400 nm). It displays strong nonlinear optical responses, with absolute SHG coefficients $|d_{22}|$ = 1.57 pm/V and $|d_{15}|$ = 0.76 pm/V. Its birefringence is sufficient to compensate for material dispersion across the entire transparent region. Theoretical analyses indicate that the π-conjugated $[C(NH_2)_3]^+$ cations dominate the SHG response. Notably, $[C(NH_2)_3]BF_4$ is identified as a full-wavelength phase-matching crystal, the first example capable of achieving phase-matched SHG across its entire optical transparency range, with the shortest PM wavelength (≈194 nm) coinciding with its UV cutoff edge. This exceptional capability arises from the pronounced anisotropy in bonding strength along different crystallographic directions, where strongly covalent $[C(NH_2)_3]^+$ units and weakly interacting $[BF_4]^-$ groups collectively yield low-dispersion refractive indices. Its full PM behavior has been experimentally demonstrated by tunable frequency-doubled output spanning 193.2–266 nm using Ti: sapphire laser systems and 355 nm-pumped nanosecond optical parametric oscillators (OPOs) as excitation sources. In addition, $[C(NH_2)_3]BF_4$ exhibits a high LIDT and low thermal expansion anisotropy: its LIDT exceeds that of *β*-BBO and KDP, while its thermal expansion anisotropy is lower than that of *β*-BBO and comparable to those of CLBO and KDP. Collectively, these outstanding properties establish $[C(NH_2)_3]BF_4$ as a highly promising candidate for UV and deep-UV NLO applications.

View Article Online
DOI: 10.1039/D6SC03331H

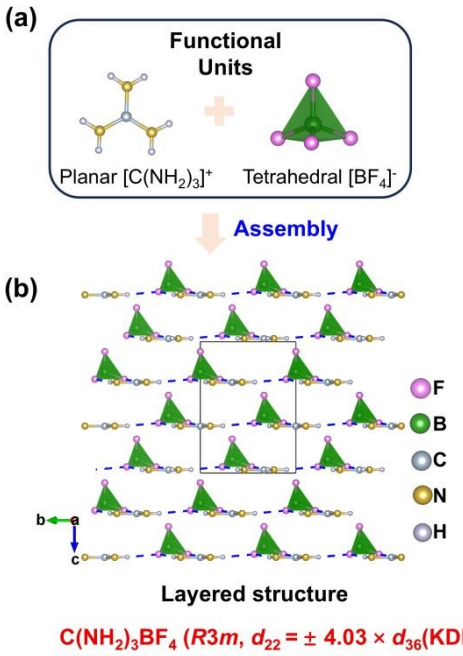

Figure 5. Crystal structure of $C(NH_2)_3BF_4$. (a) Functional building units. (b) Layered structure.

3. UV NLO crystals assembled from melamine and tetrahedral units

β-BBO is one of the most widely used UV NLO crystals, owing to its broad UV transparency (λ_{cutoff} = 189 nm), high SHG efficiency (~5.6 × KDP), sufficient birefringence (Δn = 0.122@546 nm), the feasibility of growing large single crystals, and its robust physico-chemical stability. The excellent NLO performance of *β*-BBO is closely related to its benzene-like $[B_3O_6]^{3-}$ six-membered ring (6-MR), which can be regarded as being formed by the cyclic trimerization of three $[BO_3]$ units through shared oxygen atoms. Compared to the $[BO_3]$ monomer, the polymerized $[B_3O_6]^{3-}$ unit exhibits enhanced hyperpolarizability and polarizability anisotropy, arising from its highly delocalized π-electron system. Inspired by this structural motif, several $[B_3O_6]^{3-}$-like 6-MR organic units have been developed, including $[C_3H_xN_3O_3]^{(3-x)-}$ (x = 0, 1, 2; cyanurate), $[C_3H_{6+x}N_6]^{x+}$ (x = 0, 1, 2; melamine derivatives), and $[C_3H_xN_3S_3]^{(3-x)-}$ (x = 0, 1, 2; trithiocyanate). [37-42]Among these, melamine typically forms cationic species such as $[C_3H_7N_6]^+$ (x = 1) and $[C_3H_8N_6]^{2+}$ (x = 2) under acidic conditions, enabling their effective integration with tetrahedral anions. Liu et al. theoretically investigated the microscopic properties of the monoprotonated $[C_3H_7N_6]^+$ unit and found that it exhibits higher polarizability anisotropy and hyperpolarizability than the $[B_3O_6]^{3-}$ ring, while

simultaneously maintaining a suitable UV band gap.[22]This makes it a promising building block for designing UV NLO crystals with large birefringence and strong SHG responses. Subsequently, they reported $2(C_3H_7N_6)^+ \cdot 2Cl^- \cdot H_2O$,[40] which exhibits a strong SHG response (4.3 × KDP), large birefringence (Δn = 0.277 at 546 nm), and a relatively short UV cutoff edge at 245 nm, highlighting the significant potential of melamine-based units for achieving excellent NLO performance. The discovery of $2(C_3H_7N_6)^+ \cdot 2Cl^- \cdot H_2O$ has stimulated extensive research into melamine-based UV NLO materials, particularly focusing on the incorporation of melamine-derived π-conjugated units with tetrahedral anionic groups.

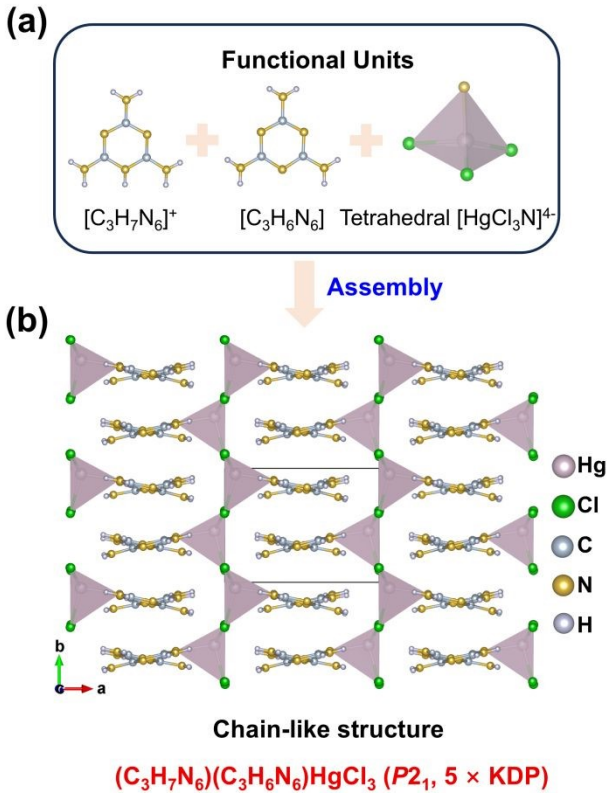

Figure 6. Crystal structure of $(C_3H_7N_6)(C_3H_6N_6)HgCl_3$. (a) Functional building units. (b) Chain-like structure.

A d^{10} cation Zn^{2+}-centered tetrahedron-based NLO crystal, $(C_3H_7N_6)(C_3H_6N_6)ZnCl_3$, was discovered by Lin and co-workers.[22] It crystallizes in the polar space group $P2_1$ and features protonated melamine ($[C_3H_7N_6]^+$) and neutral melamine ($[C_3H_6N_6]$) π-conjugated units, together with distorted $[ZnCl_3N]^{5-}$ tetrahedra. The melamine units adopt a nearly parallel arrangement along the *b*-axis, whereas the $[ZnCl_3N]^{5-}$ tetrahedra

are oriented in opposite directions, result in a negligible net contribution to the NLO response from the inorganic units. This compound exhibits a short UV cutoff edge at 236 nm, a strong SHG response (2.8 × KDP), and a large birefringence (Δn = 0.26 at 546 nm). Notably, the thermal stability of $(C_3H_7N_6)(C_3H_6N_6)ZnCl_3$ is significantly improved compared with that of $2(C_3H_7N_6)^+ \cdot 2Cl^- \cdot H_2O$ (250 °C vs. 90 °C), mainly due to the absence of crystalline water in $(C_3H_7N_6)(C_3H_6N_6)ZnCl_3$. Structure-property analyses indicate that the optical properties, particularly the SHG response and birefringence, originate predominantly from the π-conjugated melamine units, while the $[ZnCl_3N]^{5-}$ tetrahedra contribute minimally attributed to their antiparallel arrangement.

Soon after, Ok et al. further substituted Zn^{2+} with the heavier d^{10} cation Hg^{2+} and synthesized two new compounds: $(C_3H_7N_6)_3HgCl_5$ and $(C_3H_7N_6)(C_3H_6N_6)HgCl_3$.[30] The former crystallizes in the centrosymmetric (CS) space group $P1$, whereas the latter belongs to the NCS space group $P2_1$ and is isostructural with $(C_3H_7N_6)(C_3H_6N_6)ZnCl_3$(Figure 6). In $(C_3H_7N_6)(C_3H_6N_6)HgCl_3$, acentric $[HgCl_3(C_3H_6N_6)]^-$ clusters are formed via coordination of neutral melamine $[C_3H_6N_6]$ to Hg^{2+}, whereas centric $[HgCl_4]^{2-}$ tetrahedra are present in $(C_3H_7N_6)_3HgCl_5$. Notably, the melamine molecules in $(C_3H_7N_6)(C_3H_6N_6)HgCl_3$ adopt a very small dihedral angle (2.983°), and this nearly coplanar arrangement, together with the asymmetric $[HgCl_3(C_3H_6N_6)]^-$ units, leads to the formation of an NCS structure. In contrast, $(C_3H_7N_6)_3HgCl_5$ lacks Hg–N coordination and exhibits antiparallel packing of melamine, resulting in a CS structure. $(C_3H_7N_6)(C_3H_6N_6)HgCl_3$ exhibits a strong SHG response (5 × KDP) with type-**I** phase-matching behavior. It shows a UV cutoff edge at 278 nm, corresponding to a band gap of 4.40 eV, which is larger than that of the CS phase, possibly attributed to Hg–N coordination. A relatively large birefringence (Δn = 0.246 at 1064 nm) is also observed. Thermal stability studies also show that $(C_3H_7N_6)_3HgCl_5$ and $(C_3H_7N_6)(C_3H_6N_6)HgCl_3$ remain stable up to 247 °C and 225 °C, respectively. Theoretical SHG-weighted electron density analyses indicate that the SHG response arises from synergistic contributions of the melamine units (52.6%) and

View Article Online
DOI: 10.1039/D6SC03331H

the $[HgCl_3N]^{5-}$ tetrahedra (47.1%), whereas the birefringence is predominantly governed by the π-conjugated melamine units (80.1%). Interestingly, the $[ZnCl_3N]^{5-}$ tetrahedra in the Zn analogue contribute minimally to the SHG response, whereas the $[HgCl_3N]^{5-}$ tetrahedra exhibit contributions comparable to those of the melamine units. This difference can be attributed to the stronger polarizing ability of Hg^{2+} relative to Zn^{2+}, as well as the incomplete cancellation of dipole moments associated with the $[HgCl_3N]^{5-}$ units in the crystal structure. However, it should be noted that, compared with the Zn-based phase, the Hg-analogue exhibits a noticeable red shift in UV transparency, which may limit its applicability in the deep-UV region. To address this limitation, combining melamine units with tetrahedral anions that possess intrinsically wide UV transparency is a more favorable strategy. In this context, Wang et al. incorporated $[C_3H_7N_6]^+$ into deep-UV transparent sulfonate tetrahedra $[NH_2SO_3]^-$ to synthesize $[C_3H_7N_6]NH_2SO_3$, which exhibits a record-short UV cutoff edge of 206 nm and a wide optical band gap of 5.53 eV. Notably, this compound also displays a giant birefringence (Δn = 0.340 at 546 nm), surpassing that of most reported melamine-containing materials.

Although neutral $[C_3H_6N_6]$ and monovalent $[C_3H_7N_6]^+$ melamine units have been successfully integrated with diverse tetrahedral anions, the divalent $[C_3H_8N_6]^{2+}$ species had received relatively little attention until recent work by Mutailipu and co-workers.[31] In their study, the authors systematically investigated the structural features and fundamental properties of the three 6-MR units, $[C_3H_6N_6]$, $[C_3H_7N_6]^+$, and $[C_3H_8N_6]^{2+}$. They revealed that, among these, the $[C_3H_8N_6]^{2+}$ motif exhibits lower molecular symmetry, a pronounced internal push-pull electronic structure, a large permanent dipole moment, and the highest hyperpolarizability and polarizability anisotropy. These attributes render $[C_3H_8N_6]^{2+}$ a particularly promising building block for the development of high-performance UV NLO materials. By combining $[C_3H_8N_6]^{2+}$ with $[BF_4]^-$ anions, they synthesized three new compounds: NCS α-$[C_3H_8N_6](BF_4)_2{\cdot}H_2O$ and CS β-$[C_3H_8N_6](BF_4)_2{\cdot}H_2O$ and $[C_3H_8N_6](BF_4)_2{\cdot}H_2O$, all obtained via slow evaporation from aqueous solutions of melamine and HBF_4.[32] Among these, α-

$[C_3H_8N_6](BF_4)_2 \cdot H_2O$ crystallizes in the polar space group *Cc*. Its structure is composed of diprotonated melamine ($[C_3H_8N_6]^{2+}$) π-conjugated cations and tetrahedral $[BF_4]^-$ anions interconnected through an extensive hydrogen-bonding network, with water molecules serving as bridges (Figure 7). This compound exhibits a UV cutoff edge at 250 nm, corresponding to a band gap of approximately 4.55 eV. It displays a UV birefringence (Δn = 0.102 at 546.1 nm) and a strong SHG response (6.4 × KDP at 1064 nm). Moreover, efficient phase-matched 266 nm generation was demonstrated, with an output intensity approximately 1.4 times that of *β*-BBO, highlighting the capability of melamine-based materials for UV laser generation. Theoretical SHG-weighted electron density analyses indicate that the $[C_3H_8N_6]^{2+}$ cations are the dominant contributors to both the SHG response and birefringence, while the $[BF_4]^-$ anions and water molecules primarily act as structural scaffolds that enable NCS packing without diminishing the intrinsic optical properties of the cations.

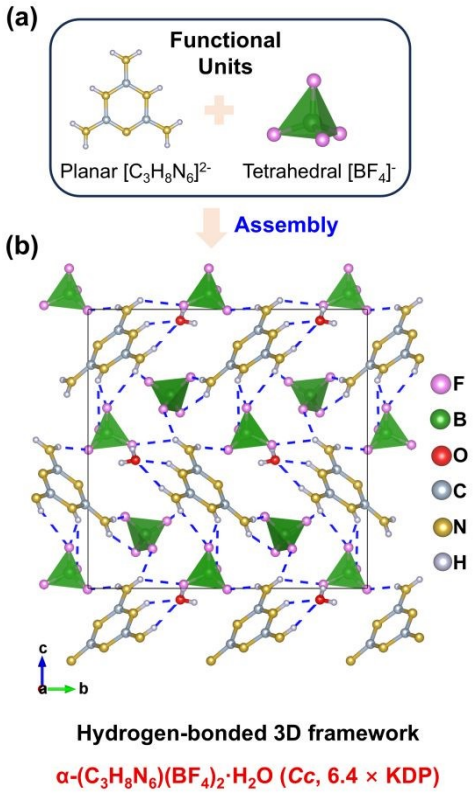

Figure 7. Crystal structure of *α*-$[C_3H_8N_6](BF_4)_2 \cdot H_2O$. (a) Functional building units. (b) Hydrogen-bonded three-dimensional framework.

4. UV NLO crystals assembled from 4-hydroxypyridine and tetrahedral units

View Article Online
DOI: 10.1039/D6SC03331H

Inspired by the successful use of guanidium and melamine units in the design of high-performance NLO crystals, increasing attention has recently been directed toward other π-conjugated building blocks. Among these, pyridine-based ions are particularly attractive owing to their tunable molecular structures and π-conjugated electronic configurations.

Chen et al. identified 4-hydroxypyridinium ($[C_5H_6ON]^+$) as a new NLO-active unit exhibiting superior polarizability anisotropy and hyperpolarizability compared with traditional inorganic building blocks.[20] However, a key challenge associated with such polar organic cations is their tendency to form CS structures owing to strong dipole-dipole interactions, which renders them NLO-inactive. To overcome this "center-symmetry-trap", the authors proposed a "salt strategy" that integrates $[C_5H_6ON]^+$ with phosphate tetrahedral anions through strong hydrogen-bonding and electrostatic interactions. By carefully controlling the protonation state of the phosphate tetrahedra to effectively screen dipole–dipole interactions, they successfully synthesized a new NLO crystal, $[C_5H_6ON]^+[H_2PO_4]^-$ (Figure 8), which crystallizes in the NCS chiral space group, $P2_12_12_1$. It is revealed that the tetrahedral $[H_2PO_4]^-$ anions act as both spatial and electrostatic buffers. Their localized yet symmetrically distributed negative charge interrupts the head-to-tail and side-by-side dipole alignment of the $[C_5H_6ON]^+$ cations. By enforcing an alternating cation–anion packing arrangement along the crystallographic axes, the anions reduce the net dipole–dipole coupling energy, thereby overcoming the energetic preference for centrosymmetric aggregation. This ‘steric–electrostatic screening’ effect is further supported by comparison with $[C_5H_6ON]_2[HPO_4]$, in which an insufficient number of anions results in residual dipole interactions and consequently a centrosymmetric structure. $[C_5H_6ON]^+[H_2PO_4]^-$ exhibits a well-balanced set of properties, including high thermal stability (decomposition temperature of 166 °C), a broad optical transparency range (0.26–1.50 μm), a strong SHG response (3 × KDP), large birefringence (Δn = 0.25), and a high LIDT (2.2 × KDP). First-principles calculations reveal that the π-conjugated $[C_5H_6ON]^+$ cation predominantly governs the optical anisotropy, while the cooperative

interaction between the organic cation and inorganic tetrahedral anion is responsible for the enhanced SHG response.

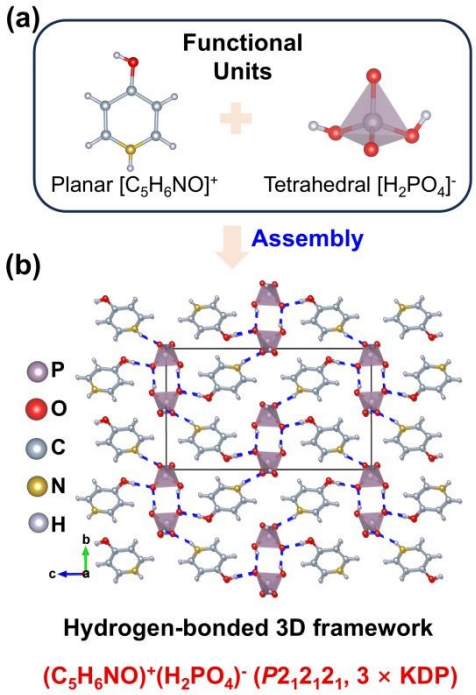

Figure 8. Crystal structure of $(C_5H_6NO)^+(H_2PO_4)^-$. (a) Functional building units. (b) Hydrogen-bonded 3D structure.

Subsequently, the tetrahedral methylsulfonate anion, $[CH_3SO_3]^-$, was also found to combine with $[C_5H_6ON]^+$, yielding 4-hydroxypyridinium methanesulfonate, $(C_5H_6ON)^+(CH_3SO_3)^-$.[32] Notably, this compound exhibits a rare heat-stimulated NLO switching behavior. Upon heating to 73 °C, partial disruption of intermolecular hydrogen bonds induces rotational reorientation of both cations and anions, triggering a phase transition from a NCS room-temperature (RTP, space group $Pna2_1$) to a CS high-temperature phase (HTP, space group $P2_1/c$). This transition is accompanied by a large thermal hysteresis of 50 °C and demonstrates reversible switching over multiple heating-cooling cycles. In the RTP phase, the crystal structure consists of π-conjugated 4-hydroxypyridinium cations and methylsulfonate anions linked via hydrogen bonds to form one-dimensional chains, which further assemble into a pseudo-two-dimensional layered motif. This phase exhibits a strong SHG response (3.3 × KDP at 1064 nm) with type-**I** phase-matching behavior, a high LIDT approximately 2.5 times that of KDP,

and a large birefringence (Δn = 0.216 at 546 nm). The UV cutoff edge is 252 nm, corresponding to a band gap of 4.64 eV, and the compound shows thermal stability up to 255 °C—the highest reported among metal-free 4-hydroxypyridinium-based materials. First-principles calculations indicate that the 4-hydroxypyridinium cation dominates both the SHG response (accounting for 82.4% of the d_{33} coefficient) and the birefringence (76.8% contribution), while the band gap arises from cooperative contributions of both the organic cation and inorganic anion.

Wu et al. have further expanded the design landscape of UV NLO crystals based on 4-hydroxypyridine by introducing a novel compound, $Zn(C_5H_4NO)_2$.[33] Uniquely, in this structure the 4-hydroxypyridine moieties function as anionic $[C_5H_4NO]^-$ ligands, rather than the conventional cationic $[C_5H_6NO]^+$ species. In contrast to typical aqueous synthesis routes, this material was prepared via a low-temperature solid-state reaction between ZnF_2 and C_5H_5NO. At 180 ℃, a thermally induced deprotonation occurs, likely following the equation:

$$2C_5H_5NO + ZnF_2 \rightarrow Zn(C_5H_4NO)_2 + 2HF\uparrow.$$

The compound crystallizes in the NCS polar space group *Fdd*2 and features an unusual heterobidentate coordination mode, in which each $[C_5H_4NO]^-$ ligand coordinates to Zn^{2+} through both N and O atoms, forming a dense 3D framework (Figure 9a-c). This rare coordination geometry ensures that all polar tetrahedral $[ZnO_2N_2]^{8-}$ units are uniformly aligned, with their dipole moments oriented along the same crystallographic direction (Figure 9d). The compound exhibits an exceptionally strong SHG response (13.6 × KDP at 1064 nm) with type-**I** phase-matching behavior. It also possesses a wide optical band gap of 4.40 eV, ensuring UV transparency. Thermal analysis indicates excellent stability up to 300 °C, along with remarkable resistance to air and moisture, maintaining both structural integrity and SHG activity after prolonged exposure. Theoretical calculations reveal that the SHG response originates predominantly from the π-conjugated $[C_5H_4NO]^-$ ligands, further enhanced by the cooperative alignment of the $[ZnN_2O_2]$ tetrahedra.

View Article Online
DOI: 10.1039/D6SC03331H

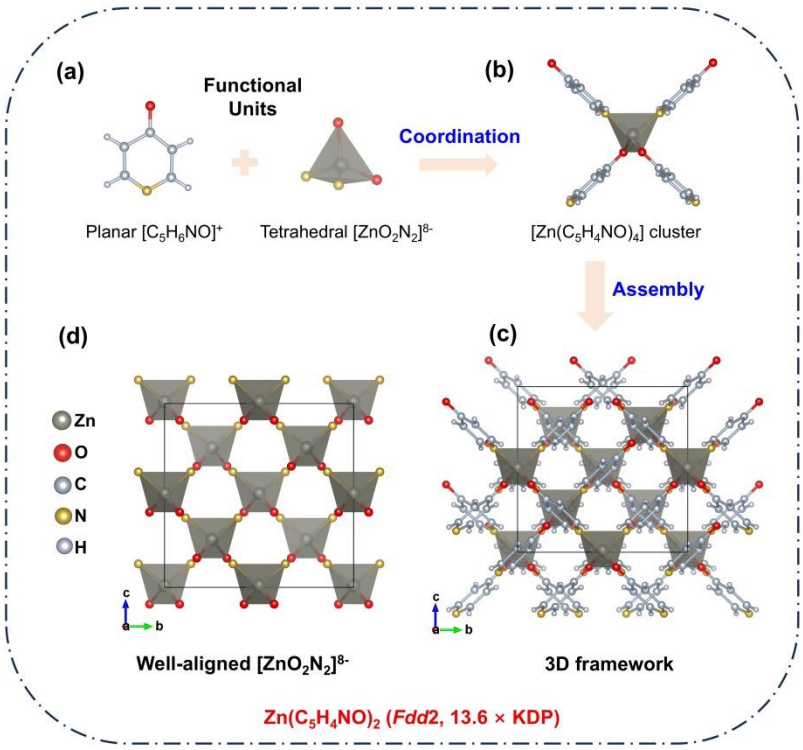

Figure 9. Crystal structure of $Zn(C_5H_4NO)_2$. (a) Functional building units. (b) $[Zn(C_5H_4NO)_4]$ cluster formed via bidentate Zn–O and Zn–N coordination. (c) 3D framework. (d) Uniformly aligned $[ZnO_2N_2]^{8-}$ tetrahedral units.

These studies demonstrate that pyridine-derived ions not only enable remarkable NLO responses but also serve as effective building blocks for achieving large birefringence, thereby motivating their broader use in the design of birefringent crystals. For instance, to overcome the intrinsically low birefringence of sulfate-based materials, Ok et al. proposed a novel "π -conjugated tailoring" strategy. By chemically modifying the $[SO_4]^{2-}$ tetrahedron, specifically, replacing one oxygen atom with a π-conjugated pyridine ring, they identified a new birefringent-active unit, 3-pyridinesulfonate ($[3\text{-}C_5H_5NSO_3]^-$). [43]This unit exhibits significantly larger polarizability anisotropy than the parent $[SO_4]^{2-}$ tetrahedron. Through crystal engineering, a series of compounds, A(3-pyridinesulfonate) (A = Li, Ag, K, Rb, Cs, NH_4), were synthesized via slow evaporation from aqueous solutions. Depending on the size and coordination behavior of the cations, the resulting structures span one-dimensional chains (Li), two-dimensional layers (Ag, Cs), and three-dimensional frameworks (K, Rb, NH_4). These materials exhibit UV

cutoff edges in the range of275–325 nm, corresponding to band gaps of 3.63–4.29 eV. Among them, K(3-$C_5H_5NSO_3$) exhibits the largest birefringence (Δn = 0.306 at 546 nm), which is approximately 16 times greater than that of KSO_3F and surpasses most reported sulfate-based materials.

The group later reported two low-dimensional compounds, [(*p*-C_5H_5NO)$ZnCl_2$] and [(*p*-C_5H_6NO)]$_2ZnCl_4$, by introducing the π-conjugated organic ligand [*p*-C_5H_5NO] into Zn-Cl frameworks.[44] The key breakthrough lies in [(*p*-C_5H_5NO)$ZnCl_2$], which exhibits a giant birefringence (Δn = 0.482 at 546 nm). This value is the highest reported among Zn-based UV birefringent materials and represents an approximately 160-fold enhancement compared with the parent $ZnCl_2$ crystal. Theoretical calculations indicate that this remarkable enhancement originates from the unique neutral [(*p*-C_5H_5NO)$ZnCl_2$]^0 clusters, which exhibit significantly higher spatial density and polarizability anisotropy than either the individual [(*p*-C_5H_6NO)]$^+$ cations or the $[ZnCl_4]^{2-}$ tetrahedra. Furthermore, the nearly coplanar arrangement of the [*p*-C_5H_5NO] molecules (with a dihedral angle of only 0.634°) maximizes the contribution of the π-conjugated system to the overall birefringence. In contrast, the [(*p*-C_5H_6NO)]$^+$ units in [(*p*-C_5H_6NO)]$_2ZnCl_4$ adopt a much larger dihedral angle (51.38°), resulting in a reduced birefringence (Δn = 0.193). Both compounds also possess wide band gaps (4.29–4.52 eV) and short UV cutoff edges (261–275 nm), making them promising candidates for UV birefringent applications.

5. Summary and outlook

Organic π-conjugated units provide large polarizability anisotropy and high hyperpolarizability, which are essential for achieving strong SHG responses and large birefringence. Tetrahedral units, on the other hand, offer broad UV transparency and low optical dispersion, while also serving as structural directors that regulate the spatial arrangement of π-conjugated units. The cooperative integration of these complementary building blocks effectively overcomes the long-standing trade-off between wide UV transparency and high NLO efficiency, as well as sufficient birefringence, thereby providing a powerful strategy for the discovery of advanced UV NLO materials. In this

Perspective, we have systematically examined recent advances in the design and synthesis of three representative families of UV NLO materials. These systems are constructed through the integration of organic π-conjugated units (e.g., guanidinium, melamine, and 4-hydroxylpyridine) with various tetrahedral building blocks. We have highlighted their key structural motifs, functional units, crystal structures, optical properties, and underlying structure-property relationships.

The triangular guanidinium ($[C(NH_2)_3]^+$) unit is one of the most widely used organic π-conjugated motifs in the design of UV NLO materials. Structurally analogous to inorganic planar units (e.g., $[BO_3]^{3-}$), it possesses a delocalized electronic structure that gives rise to large hyperpolarizability and polarizability anisotropy. In addition, its high aqueous solubility facilitates the formation of hydrogen-bonded ionic crystals with a wide range of tetrahedral anions via facile solution-based methods. Indeed, most commonly used tetrahedral units, including fluorine-containing species ($[SO_3F]^-$, $[PO_3F]^{2-}$, $[BF_4]^-$) and non-fluorinated analogues ($[PO_4]^{3-}$, $[AsO_4]^{3-}$, and $[VO_4]^{3-}$), can be readily combined with guanidinium. In contrast, the incorporation of isolated $[BO_4]^{5-}$ and $[SiO_4]^{4-}$ tetrahedra has not yet been realized, possibly because of synthetic challenges: borates tend to form frameworks, whereas silicates are typically insoluble in aqueous media. From a structural standpoint, the nature of the tetrahedral anion strongly influences the arrangement of guanidinium units. Monovalent anions such as $[SO_3F]^-$ and $[BF_4]^-$ promote highly coplanar alignment, whereas di- and trivalent anions ($[PO_3F]^{2-}$, $[PO_4]^{3-}$, $[AsO_4]^{3-}$, and $[VO_4]^{3-}$) generally lead to more disordered orientations of the guanidinium groups. Notably, $C(NH_2)_3BF_4$ has emerged as a leading candidate for generating 266 nm coherent light. It combines a wide UV transparency range with a cutoff edge down to 193 nm, a large SHG response (~ 5 × KDP) comparable to *β*-BBO, and full-wavelength phase-matching capability across its entire transmission window, enabled by sufficient birefringence and low material dispersion. In addition, it exhibits favorable physicochemical stability and can be grown as large bulk single crystals. Beyond guanidinium, melamine and 4-hydroxypyridine units, both featuring more retentively delocalized π-electron systems, serve as highly effective motifs for

View Article Online
DOI: 10.1039/D6SC03331H

achieving enhanced NLO performance. For example, the melamine-based crystal of $C_3H_8N_6(BF_4)_2 \cdot H_2O$ exhibits a strong SHG response comparable to β-BBO and is phase-matchable at 532 nm, underscoring its potential as a fourth harmonic generation material. Similarly, 4-hydroxylpyridine-based systems demonstrate exceptional performance; notably, $Zn(C_5H_4NO)_2$ exhibits a remarkably high SHG response (13.6 × KDP), more than twice that of β-BBO.

From an application perspective, guanidinium-based NLO materials appear more competitive than their melamine- and 4-hydroxypyridine-based counterparts for several reasons. First, guanidinium-based UV NLO materials typically exhibit broader UV transmission windows. Notably, some guanidinium-based compounds remain transparent down to the deep-UV region (e.g., 193 nm for $C(NH_2)_3BF_4$), whereas melamine- and 4-hydroxypyridine-based NLO materials generally do not exhibit cutoff edges below 200 nm and instead show red-shifted absorption edges. This extended transparency range not only broadens the accessible spectral window and enables shorter-wavelength coherent light generation, but also helps reduce material dispersion. Second, for UV NLO applications, moderate birefringence (typically ~0.05–0.1) is generally preferred over excessively large values. Overly large birefringence can induce significant beam walk-off, thereby reducing frequency-conversion efficiency. This effect is well illustrated by the β-BBO crystal, which exhibits a birefringence of approximately 0.122@ 532 nm and suffers from pronounced walk-off. Among the three material families discussed here, guanidinium possesses the lowest polarizability anisotropy, resulting in more suitable birefringence values. For example, $C(NH_2)_3BF_4$ exhibits a birefringence of 0.120 at 546 nm, which is close to the optimal range for UV applications. In contrast, the stronger π-conjugation in melamine and 4-hydroxypyridine typically results in larger birefringence values ($\Delta n > 0.2$). Finally, it is noteworthy that the SHG responses of guanidinium-based compounds are generally comparable to those of melamine- and 4-hydroxypyridine-based systems, despite the intrinsically higher hyperpolarizability of the latter. This indicates that the overall second-order NLO performance of guanidinium-based materials is not inferior to that

View Article Online
DOI: 10.1039/D6SC03331H

of the other two families. Nevertheless, this does not diminish the significance of exploring melamine- and 4-hydroxypyridine-based UV NLO materials. From a chemical perspective, guanidinium offers a relatively limited design space, as it predominantly functions as a cation that assemble with anionic tetrahedral (or other anionic) groups to form hydrogen-bonded ionic crystals. In contrast, melamine and 4-hydroxypyridine exhibit greater versatility: they can act as cations, neutral molecules, or even anions, and can coordinate with metal cations to form molecular or covalently bonded 3D frameworks. This flexibility significantly enriches structural diversity and provides broader opportunities for tuning optical and physicochemical properties. With respect to guanidinium, although derivatives (e.g., $[C_2H_7N_4O]^+$) have been explored, current efforts largely focus on enhancing π-conjugation to achieve higher SHG responses and large birefringence. However, such enhancement inevitably leads to a reduction in optical band gap. Therefore, the development of guanidinium-derived functional groups with moderated π-conjugation, such as reducing the extent of conjugation by removing one amino group or introducing non-π-conjugated substituents at the periphery of the guanidinium unit, while maintaining strong NLO responses and wide transparency windows, represents a promising direction for future research. Notably, this design principle can also be extended to melamine- and 4-hydroxylpridine-based systems.

Author contributions

Conceptualization: K. M. Ok, J. Luo; original draft: Z. Bai; review and editing: all authors; funding acquisition: K. M. Ok, J. Luo, and Z. Bai.

Conflicts of interest

The authors declare no conflicts of interest.

Data availability

No new data were generated or analyzed as part of this perspective.

Acknowledgement

View Article Online
DOI: 10.1039/D6SC03331H

This work was supported by the National Research Foundation of Korea (NRF), funded by the Ministry of Science and ICT (Grant No. RS-2024-00442105). We also gratefully acknowledge the National Natural Science Foundation of China (22193042, 22505280), and the Natural Science Foundation of Fujian Province (2025J08119).

Notes and references

1. M. Mutailipu, K. R. Poeppelmeier and S. Pan, *Chem. Rev.*, 2021, **121**, 1130-1202.
2. T. Wu, X. Jiang, C. Wu, Y. Hu, Z. Lin, Z. Huang, M. G. Humphrey and C. Zhang, *Angew. Chem. Int. Ed.*, 2022, **61**, e202203104.
3. C. Wu, C. Jiang, G. Wei, X. Jiang, Z. Wang, Z. Lin, Z. Huang, M. G. Humphrey and C. Zhang, *J. Am. Chem. Soc.*, 2023, **145**, 3040-3046.
4. Y. Hu, C. Wu, X. Jiang, K. Duanmu, Z. Huang, Z. Lin, M. G. Humphrey and C. Zhang, *Angew .Chem. Int. Ed.*, 2023, **62**, e202315133.
5. X. Dong, H. Huang, L. Huang, Y. Zhou, B. Zhang, H. Zeng, Z. Lin and G. Zou, *Angew. Chem. Int. Ed.*, 2024, **63**, e202318976.
6. C. Chen, B. Wu, A. Jiang and G. You, *Sci. Sin., Ser. B*, 1985, **28**, 235-243.
7. C. Chen, Y. Wu, A. Jiang, B. Wu, G. You, R. Li and S. Lin, *J. Opt. Soc. Am. B*, 1989, **6**, 616-621.
8. X. Zhu, H. Tu, Y. Zhao and Z. Hu, *Crystals*, 2017, **7**, 83.
9. Y. Wu, T. Sasaki, S. Nakai, A. Yokotani, H. Tang and C. Chen, *Appl. Phys. Lett.*, 1993, **62**, 2614-2615.
10. C. T. Chen, G. L. Wang, X. Y. Wang and Z. Y. Xu, *Appl. Phys. B*, 2009, **97**, 9-25.

View Article Online
DOI: 10.1039/D6SC03331H

11. M. Mutailipu, M. Zhang, H. Wu, Z. Yang, Y. Shen, J. Sun and S. Pan, *Nat. Commun.*, 2018, **9**, 3089.

12. G. Shi, Y. Wang, F. Zhang, B. Zhang, Z. Yang, X. Hou, S. Pan and K. R. Poeppelmeier, *J. Am. Chem. Soc.*, 2017, **139**, 10645-10648.

13. F. Zhang, Z. Chen, C. Cui, Z. Yang, M. Mutailipu, F. Li, X. Hou, X. Long and S. Pan, *Nature*, 2026, https://doi.org/10.1038/s41586-025-10007-z.

14. J. Zhou, Y. Liu, H. Wu, H. Yu, Z. Lin, Z. Hu, J. Wang and Y. Wu, *Angew. Chem. Int. Ed.*, 2020, **59**, 19006-19010.

15. G. Peng, C. Lin and N. Ye, *J. Am. Chem. Soc.*, 2020, **142**, 20542-20546.

16. J. Huang, C. Zhang, S. Chen and A. Abudurusuli, *Coord. Chem. Rev.*, 2025, **536**, 216632.

17. Z. Chen, C. Li, B. Yang, J. Lu, Z. Yang, J. Li, X. Hou, S. Pan and M. Mutailipu, *Angew. Chem. Int. Ed.*, 2026, **65**, e8834948.

18. Z. Chen, C. Li, X. Wu, J. Lu, Z. Yang, X. Hou and M. Mutailipu, *Aggregate*, 2025, **6**, e70134.

19. Z. Bai, S. Zhao, K. M. Ok and J. Luo, *Chin. J. Struct. Chem.*, 2026, **45**, 100802.

20. J. Lu, X. Liu, M. Zhao, X. B. Deng, K. X. Shi, Q. R. Wu, L. Chen and L. M. Wu, *J. Am. Chem. Soc.*, 2021, **143**, 3647-3654.

21. X. Wen, Y. Yan, J. Lu, X. Shi, P. Tang, J. Chen, G. Yang, G. Peng, H. Yu, H. Zhang, Z. Hu, J. Wang and N. Ye, *Angew. Chem. Int. Ed.*, 2025, **64**, e202424153.

22. L. Liu, Z. Bai, L. Hu, D. Wei, Z. Lin and L. Zhang, *J. Mater. Chem. C*, 2021, **9**, 7452-7457.

View Article Online
DOI: 10.1039/D6SC03331H

23. H. Tian, C. Lin, X. Zhao, F. Xu, C. Wang, N. Ye and M. Luo, *CCS Chem.*, 2023, **5**, 2497-2505.

24. M. Mutailipu and S. Pan, *Angew. Chem. Int. Ed.*, 2020, **59**, 20302-20317.

25. M. Luo, C. Lin, D. Lin and N. Ye, *Angew. Chem. Int. Ed.*, 2020, **59**, 15978-15981.

26. C. Jin, H. Zeng, F. Zhang, H. Qiu, Z. Yang, M. Mutailipu and S. Pan, *Chem. Mater.*, 2021, **34**, 440-450.

27. C. Wu, X. Jiang, Z. Wang, H. Sha, Z. Lin, Z. Huang, X. Long, M. G. Humphrey and C. Zhang, *Angew. Chem. Int. Ed.*, 2021, **60**, 14806-14810.

28. G. Xu, X. Bai, Z. Yang, J. Han and S. Pan, *Angew. Chem. Int. Ed.*, 2025, **64**, e202510363.

29. M. Mutailipu, J. Han, Z. Li, F. Li, J. Li, F. Zhang, X. Long, Z. Yang and S. Pan, *Nat. Photonics*, 2023, **17**, 694-701.

30. Z. Bai, J. Lee, H. Kim, C. L. Hu and K. M. Ok, *Small*, 2023, **19**, 2301756.

31. X. Long, F. Li, H. Qiu, X. Hou, J. Lu, J. Li, Z. Yang, J. Cao, S. Pan and M. Mutailipu, *Angew. Chem. Int. Ed.*, 2026, **65**, e22210.

32. Z. P. Zhang, X. Liu, R. X. Wang, S. Zhao, W. J. He, H. Y. Chen, X. B. Deng, L. M. Wu, Z. Zhou and L. Chen, *Angew. Chem. Int. Ed.*, 2024, **63**, e202408551.

33. C. Yang, J. Gou, Y. Zhu, Y. Xiong, Z. Zhu, L. Chen and Q. Wu, *Angew. Chem. Int. Ed.*, 2025, **64**, e202420810.

34. L. Xiong, J. Chen, J. Lu, C.-Y. Pan and L.-M. Wu, *Chem. Mater.*, 2018, **30**, 7823-7830.

View Article Online
DOI: 10.1039/D6SC03331H

35. D. Wang, Z. Wei, Z. Bai, L. Liu, Z. Lin and L. Zhang, *Dalton Trans.*, 2022, **51**, 463-467.

36. Z. Bai, Y. Kuk, J. Lee, H. Kim and K. M. Ok, *Inorg. Chem.*, 2024, **63**, 3578-3585.

37. J. Lu, Lian, Y. K., Xiong, L., Wu, Q. R., Zhao, M., Shi, K. X., Wu, L. M. , *J. Am. Chem. Soc.*, 2019, **141**, 16151-16159.

38. D. Lin, M. Luo, C. Lin, F. Xu and N. Ye, *J. Am. Chem. Soc.*, 2019, **141**, 3390-3394.

39. M. Kalmutzki, M. Strobele, F. Wackenhut, A. J. Meixner and H. J. Meyer, *Angew. Chem. Int. Ed.*, 2014, **53**, 14260-14263.

40. L. Liu, C. L. Hu, Z. Bai, F. Yuan, Y. Huang, L. Zhang and Z. Lin, *Chem. Commun.*, 2020, **56**, 14657-14660.

41. Q. Xu, Y. Liu, Q. Wu, L. Hou, Y. Li, L. Li, Z. Lin, S. Zhao and J. Luo, *Sci. China Mater.*, 2023, **66**, 3271-3277.

42. M. Li, X. Zhang, Z. Xiong, Y. Li, Y. Zhou, X. Chen, Y. Song, M. Hong, J. Luo and S. Zhao, *Angew. Chem. Int. Ed.*, 2022, **61**, e202211151.

43. Z. Bai and K. M. Ok, *Angew. Chem. Int. Ed.*, 2023, **63**, e202315311.

44. Y. Li and K. M. Ok, *Angew .Chem. Int. Ed.*, 2024, **63**, e202409336.

View Article Online
DOI: 10.1039/D6SC03331H

SOGANG UNIVERSITY

Kang Min Ok
Professor

T: +82-2-705-7959
E: kmok@sogang.ac.kr

April 21, 2026

Hybridizing π-conjugated organic systems with tetrahedral units: a design paradigm for advanced UV nonlinear optical materials

Data availability Statement

No new data were generated or analyzed as part of this perspective.